The custodial symmetry protects the above relation from large radiative corrections. All corrections to the ρ parameter are therefore proportional to terms that break the custodial symmetry. For instance, radiative corrections involving the Higgs boson are proportional to $\sin^2\theta_W$, $\delta\rho = -11 G_F m_Z^2 \sin^2\theta_W \log(m_H^2/m_Z^2)/(24\sqrt{2}\pi^2)$, and vanish in the limit $g' \to 0$. Since $m_t \neq m_b$, there are also relevant radiative corrections generated by massive fermions. They are proportional to $m_t^2 + m_b^2 - 2(m_t^2 m_b^2)\log(m_t^2/m_b^2)/(m_t^2 - m_b^2)$ and would indeed vanish for $m_t = m_b$ [25].

11.2.3 *Stability of the Higgs potential*

The discovery of the Higgs boson with $m_H \approx 125$ GeV has far reaching consequences within the SM framework. In particular, the precise value of m_H determines the value of the quartic coupling λ at the electroweak scale and makes it possible to study its behavior up to high energy scales. A larger value of m_H would have implied that the self coupling λ would become non-perturbative at some scale Λ that could be well below the Planck scale [26].

However, for the value of Higgs boson mass experimentally measured, the EW vacuum of the Higgs potential is most likely metastable [27]. The high-energy evolution of λ shows that it becomes negative at energies $\Lambda = \mathcal{O}(10^{11})$ GeV (even though λ could remain positive till higher energy, maybe all the way to the Planck scale, if the top quark mass exceeds its current measured value by 3σ). When this occurs, the SM Higgs potential develops an instability and the long term existence of the EW vacuum is challenged. This behaviour may call for new physics at an intermediate scale before the instability develops, i.e., below M_{Planck}, even though new physics at M_{Planck} could influence the stability of the EW vacuum and possibly modify this conclusion [28]. The consequences of the instability of the EW vacuum on high-scale inflation have been discussed in Ref. [29]. It was also noticed that Higgs field fluctuations during inflation could seed the formation of primordial black holes, possibly making up the Dark Matter relic abundance [30] or they could produce a stochastic background of gravitational waves with characteristic structures [31], offering a probe of the EW vacuum near criticality.

The lifetime of the EW metastable vacuum is determined by the rate of quantum tunnelling from this vacuum into the true vacuum of the theory (for the most recent computation of the EW vacuum lifetime within the SM, see Ref. [32]). Within the SM, the running of the Higgs self coupling slows down at high energies with a cancellation of its β-function at energies just one to two orders of magnitude below the Planck scale [33]. This slow evolution of the quartic coupling is responsible for saving the EW vacuum from premature collapse. It might also help the Higgs boson to play the role of an inflaton [34] (see, however, Ref. [35] for potential issues with this Higgs-boson-as-an-inflaton idea).

11.2.4 *Higgs boson production and decay mechanisms*

Comprehensive reviews of the SM Higgs boson properties and phenomenology, with an emphasis on the impact of loop corrections to the Higgs boson decay rates and cross sections, can be found in Refs. [36–40]. The main results are summarised here.

11.2.4.1 *Production mechanisms at hadron colliders*

The main production mechanisms at the Tevatron collider and the LHC are gluon fusion (ggF), weak-boson fusion (VBF), associated production with a gauge boson (VH), and associated production with a $t\bar{t}$ pair ($t\bar{t}H$) or with a single top quark (tHq). Figure 11.1 depicts representative diagrams for these dominant Higgs boson production processes.

The state-of-the-art of the theoretical calculations in the main different production channels is summarised in Table 11.1.

The cross sections for the production of a SM Higgs boson as a function of $\sqrt{s}$, the center of mass energy, for pp collisions, including bands indicating the theoretical uncertainties, are summarised

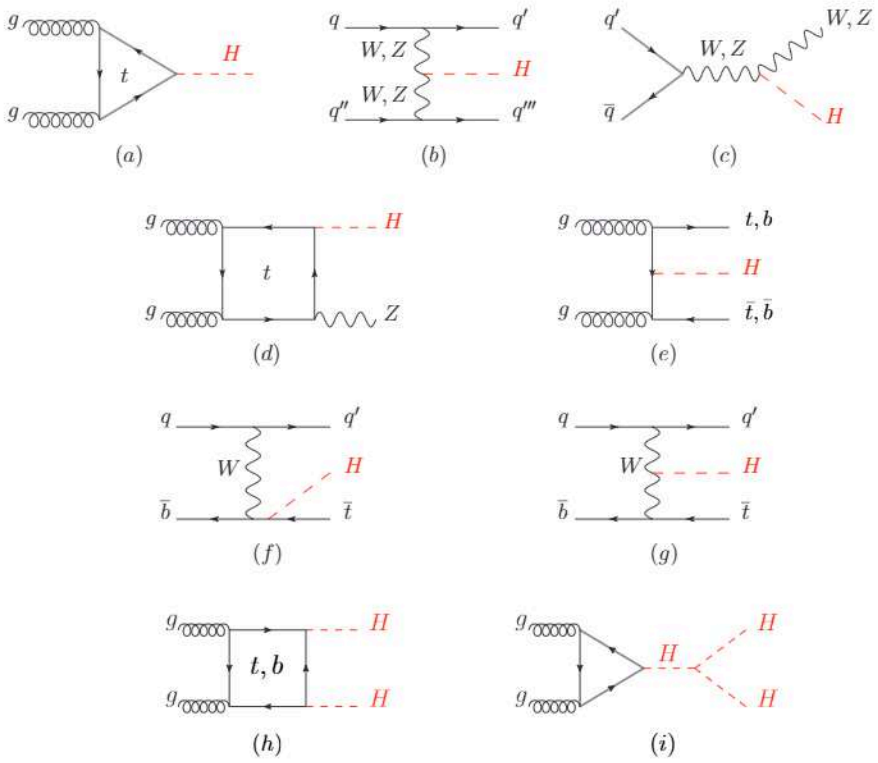

Figure 11.1: Main leading order Feynman diagrams contributing to the single Higgs boson production in (*a*) gluon fusion, (*b*) Vector-boson fusion, (*c*) Higgs-strahlung (or associated production with a gauge boson at tree level from a quark-quark interaction), (*d*) associated production with a gauge boson (at loop level from a gluon-gluon interaction), (*e*) associated production with a pair of top/bottom quarks, (*f*-*g*) production in association with a single top quark, and double Higgs production through (*h*) a top- and bottom-quark loop, (*i*) the self coupling of the Higgs boson.

in Fig. 11.2 (left) [43]. A detailed discussion, including uncertainties in the theoretical calculations due to missing higher-order effects and experimental uncertainties on the determination of SM parameters involved in the calculations, can be found in Refs. [37–40]. These references also contain state-of-the-art discussions on the impact of PDF uncertainties, QCD scale uncertainties and uncertainties due to different procedures for including higher-order corrections matched to parton shower simulations, as well as uncertainties due to hadronisation and parton-shower events.

Table 11.2 summarises the Higgs boson production cross sections and relative uncertainties for a Higgs boson mass of 125 GeV, for $\sqrt{s} = 7$, 8, 13, 13.6 and 14 TeV.

i. *Gluon fusion production mechanism*

At high-energy hadron colliders, the Higgs boson production mechanism with the largest cross section is the gluon-fusion process, $gg \to H + X$, mediated by the exchange of a virtual, heavy top quark [45]. Contributions from lighter quarks propagating in the loop are suppressed proportionally to m_q^2. QCD radiative corrections to the gluon-fusion process are very important and have been studied in detail. Including the full dependence on the (top, bottom, charm) quark and Higgs boson masses, the cross section has been calculated at the next-to-leading order (NLO) in α_s [46,47]. To a very good approximation, the leading top-quark contribution can be evaluated in the limit $m_t \to \infty$ by matching the SM to an effective theory. The gluon-fusion amplitude is then evaluated from an

Table 11.1: State-of-the-art of the theoretical calculations in the main Higgs boson production channels in the SM, and, when publicly available, the major MC tools used in the simulations. Furthermore, all the Higgs-boson production modes have been interfaced with parton-shower event generators at NLO QCD like `Poweg-Box, MG5_aMC@NLO or Sherpa` (the entries "—" indicate cases when the results are implemented in codes that are not yet public). For ggF and VH NNLO matched simulations now also exist. Differential NNLO QCD results exist for $t\bar{t}H$ [41] (though the exact 2-loop virtual corrections are still missing) and have been implemented in `MATRIX` [42].

ggF	VBF	VH	$t\bar{t}H$
Inclusive:	Inclusive:	Inclusive:	Inclusive:
N3LO QCD + NLO EW	N3LO QCD	N3LO QCD	NNLO QCD
`(iHixs)`	`proVBFH`	`(n3loxs)`	—
N3LO QCD		NNLO QCD	
`ggHiggs`		`(VH@NNLO)`	
Differential:	Differential:	Differential:	Differential:
NNLO+N3LL QCD	NNLO QCD	NNLO QCD	NLO QCD+EW
`(Radish+NNLOJET)`	—	—	`(MG5_aMC@NLO)`
N3LO+N3LL′ QCD	NLO QCD + EW	NLO QCD + EW	
`(TROLL)`	`(HAWK)`	`(HAWK)`	

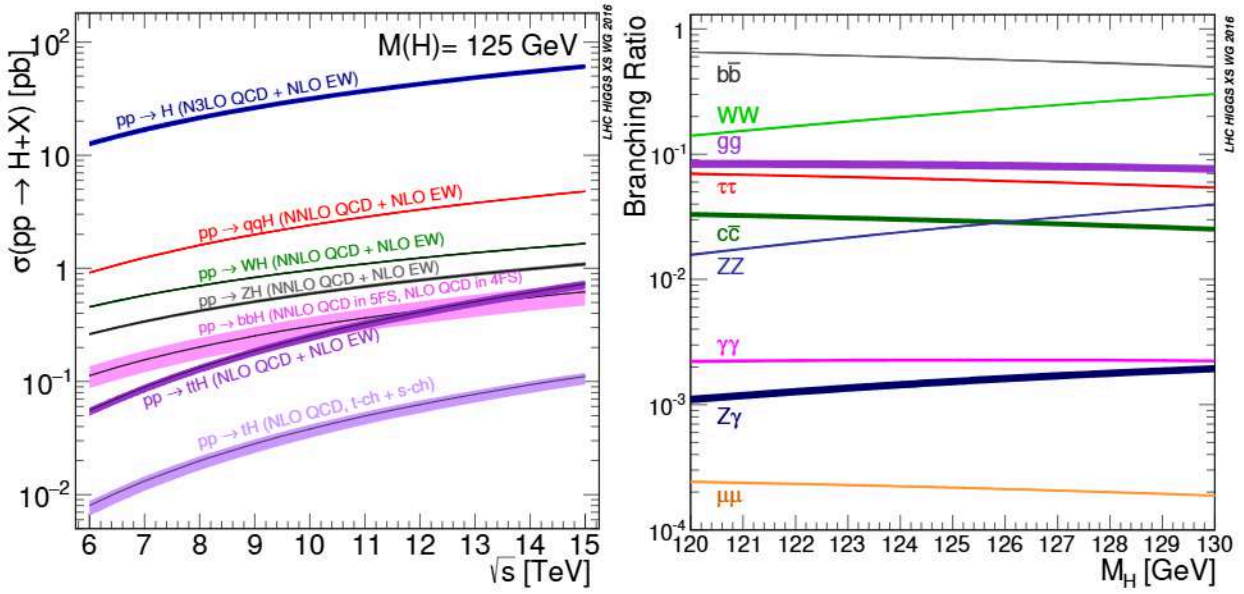

Figure 11.2: (Left) The SM Higgs boson production cross sections as a function of the center of mass energy, $\sqrt{s}$, for pp collisions [43]. The VBF process is indicated here as qqH. (Right) The branching ratios for the main decays of the SM Higgs boson near $m_H = 125\,\text{GeV}$ [39, 40]. The theoretical uncertainties are indicated as bands.

effective Lagrangian containing a local $HG^a_{\mu\nu}G^{a\,\mu\nu}$ operator [21, 22]. In this approximation, the cross section is known at next-to-next-to-next-to-leading order in α_s expansion (N3LO QCD) [48]. The validity of the effective theory with infinite m_t is greatly enhanced by rescaling the result by the exact LO result: $\sigma = (\sigma^{\text{LO}}_{m_t}/\sigma^{\text{LO}}_{m_t=\infty}) \times \sigma_{m_t=\infty}$ [40]. The large top-quark mass approximation, after

Table 11.2: The SM Higgs boson production cross sections for $m_H = 125\,\text{GeV}$ in pp collisions ($p\bar{p}$ collisions at $\sqrt{s} = 1.96\,\text{TeV}$ for the Tevatron), as a function of the center of mass energy, $\sqrt{s}$. The predictions for the LHC energies are taken from Refs. [37–40, 43], the ones for the Tevatron energy are the ones used in Ref. [44]. The predictions for the ggF channel at the LHC include the latest N3LO QCD + NLO EW results. The uncertainties are estimated assuming no correlation between α_S and PDF uncertainties. The uncertainties on the total cross sections are dominated by the ones on the gluon fusion process.

$\sqrt{s}$ (TeV)	Production cross section (in pb) for $m_H = 125\,\text{GeV}$					
	ggF	VBF	WH	ZH	$t\bar{t}H$	total
1.96	$0.95^{+17\%}_{-17\%}$	$0.065^{+8\%}_{-7\%}$	$0.13^{+8\%}_{-8\%}$	$0.079^{+8\%}_{-8\%}$	$0.004^{+10\%}_{-10\%}$	$1.23^{+15\%}_{-15\%}$
7	$16.9^{+5.5\%}_{-7.6\%}$	$1.24^{+2.2\%}_{-2.2\%}$	$0.58^{+2.2\%}_{-2.3\%}$	$0.34^{+3.1\%}_{-3.0\%}$	$0.09^{+5.6\%}_{-10.2\%}$	$19.1^{+5\%}_{-7\%}$
8	$21.4^{+5.4\%}_{-7.6\%}$	$1.60^{+2.1\%}_{-2.1\%}$	$0.70^{+2.1\%}_{-2.2\%}$	$0.42^{+3.4\%}_{-2.9\%}$	$0.13^{+5.9\%}_{-10.1\%}$	$24.2^{+5\%}_{-7\%}$
13	$48.6^{+5.6\%}_{-7.4\%}$	$3.78^{+2.1\%}_{-2.1\%}$	$1.37^{+2.0\%}_{-2.0\%}$	$0.88^{+4.1\%}_{-3.5\%}$	$0.50^{+6.8\%}_{-9.9\%}$	$55.1^{+5\%}_{-7\%}$
13.6	$52.2^{+5.6\%}_{-7.4\%}$	$4.1^{+2.1\%}_{-1.5\%}$	$1.46^{+1.8\%}_{-1.9\%}$	$0.95^{+4.0\%}_{-3.6\%}$	$0.57^{+6.9\%}_{-9.9\%}$	$59.2^{+5\%}_{-7\%}$
14	$54.7^{+5.6\%}_{-7.4\%}$	$4.28^{+2.1\%}_{-2.1\%}$	$1.51^{+1.8\%}_{-1.9\%}$	$0.99^{+4.1\%}_{-3.7\%}$	$0.61^{+6.9\%}_{-9.8\%}$	$62.1^{+5\%}_{-7\%}$

this rescaling of the cross section, yields a next-to-next-to-leading order (NNLO) QCD result that has been established to be at the percent level accuracy [49]. Further progress was made to include full top mass dependence at NNLO QCD [50]. And the bottom and light quark contributions to the Higgs production have been reassessed in Refs. [51–53].

The LO contribution and NLO QCD corrections [54] amount to about 80% of the total N3LO QCD cross section. The NNLO QCD corrections [55] further enhance the cross section by approximately 30% of the LO plus NLO result (at $\mu_f = \mu_r = m_H/2$). Electroweak radiative corrections have been computed at NLO and increase the LO cross section by about 5% for $m_H \simeq 125\,\text{GeV}$ [56]. Mixed QCD-EW corrections are now being investigated with encouraging results on the computation of the exact 3-loop amplitude [57] complementing the results obtained in either limit of heavy [58] or massless [59] gauge bosons. The mixed QCD-EW corrections still have to be evaluated at large p_T.

At N3LO QCD, the perturbation series is rather stable with a mere enhancement of 3% of the total cross section, with a central value quite insensitive to threshold resummation effects with the scale choice mentioned above ($\mu_f = \mu_r = m_H/2$) [40, 48, 60, 61]. At the LHC with a center-of-mass energy of 13 TeV, the most up-to-date value for the production cross section of a 125 GeV Higgs boson amounts to [40]

$$\sigma^{\text{N3LO}}_{\text{ggF}} = 48.6\,^{+2.2\,(4.6\%)}_{-3.3\,(6.7\%)}\,(\text{theory}) \pm 1.6\,(3.2\%)\,(\text{PDF} + \alpha_s)\,\text{pb}. \tag{11.10}$$

This cross-section was first computed in terms of an expansion around the production threshold of the Higgs boson. This approximation was overcome in Ref. [61]. The PDF uncertainty of order 1-2% quoted above has been questioned as the first global analysis of PDFs at approximate N3LO

QCD was presented, suggesting an unexpected decrease of the cross-section central value by more than 5% [62].

Besides considering the inclusive Higgs boson production cross section at the LHC, it is important to study differential distributions in order to probe the properties of the Higgs boson in a detailed way. The Higgs boson rapidity distribution has been computed at the N3LO QCD order in Ref. [63]. And fully differential N3LO QCD predictions for Higgs production in gluon fusion have been obtained by combining N3LO QCD predictions for Higgs rapidity distribution with NNLO QCD predictions for H+jet [64]. A more exclusive account of Higgs boson production is also required because experimental analyses often impose cuts on the final states in order to improve the signal-to-background ratio. Using soft-collinear effective theory, large fiducial power corrections induced by fiducial cuts have been resummed at N3LO+N3LL$'$ QCD accuracy, i.e. at next-to-next-to-next-leading-log, incorporating the complete $\mathcal{O}(\alpha_s^3)$ singular structure for $q_T \to 0$ allowing one to consistently match to N3LO QCD [65]. This is the most accurate result that can be directly compared with fiducial measurements. Different fiducial cuts are explored to suppress these fiducial effects. In addition, progress has been made to improve the calculation of the Higgs boson production cross section with a jet veto (the "0-jet bin" or in the presence of a veto bounding the transverse momentum of the hardest accompanying jet) [66], reaching NNLL accuracy matched to N3LO QCD. These accurate predictions for the jet-veto cross section are required, e.g., to suppress the $t\bar{t}$ background in the $H \to WW$ channel [67].

ii. *Vector boson fusion production mechanism*

The SM Higgs boson production mode with the second-largest cross section at the LHC is vector boson fusion. At the Tevatron collider, VBF also occurred, but for $m_H = 125\,\text{GeV}$ had a smaller cross section than Higgs boson production in association with a W or Z boson. Higgs boson production via VBF, $qq \to qqH$, proceeds by the scattering of two (anti-)quarks, mediated by t- or u-channel exchange of a W or Z boson, with the Higgs boson radiated off the weak-boson propagator. The scattered quarks give rise to two hard jets in the forward and backward regions of the detector with a large rapidity gap [68]. Because of the color-singlet nature of the weak-gauge boson exchange, gluon radiation from the central-rapidity regions is strongly suppressed. These characteristic features of VBF processes can be exploited to distinguish them from overwhelming QCD backgrounds, including gluon-fusion induced Higgs boson + 2 jet production, and from s-channel WH or ZH production with a hadronically decaying weak gauge boson. After the application of specific selection cuts, the VBF channel provides a clean environment, not only for the Higgs boson searches originally performed, but also for the subsequent determination of Higgs boson couplings at the LHC.

The cross-section is known at N3LO QCD at the inclusive level [69] and at NNLO enforcing the VBF cuts [70] with a residual uncertainty of the order of few permill. However, this result is obtained in the DIS/factorized approximation [71] where the fusing gauge bosons are emitted from the two quark legs independently. While, the exact NNLO QCD VBF calculation will remain out-of-reach in the near future, the leading non-factorisable contributions with two forward jets have been estimated [72] and the impact of non-factorizable effects have been studied in Ref. [73]. They give some corrections, also of the order of few permill, to inclusive quantities, but they are an order of magnitude larger for differential observables. Overall, the residual uncertainty is of the order of a few percent but is quite sensitive to the tagging jet cuts and jet radius modelling [74]. Extensive studies on VBF at fixed order and with parton shower matched computations can be found in Ref. [75]. In addition, EW corrections have been included and the VBF process is known at NLO QCD+EW order for some time [76, 77].

iii. *WH and ZH associated production mechanism*

The next most relevant Higgs boson production mechanisms are associated production with W and Z gauge bosons. The cross sections for the associated production processes, $pp \to VH + X$, with $V = W^{\pm}, Z$ receive contributions at NLO QCD given by NLO QCD corrections to the Drell–Yan cross section [78,79] and from NLO EW corrections. The latter, unlike the QCD corrections, do not respect the factorisation into Drell–Yan production since there are irreducible box contributions already at one loop [76,80]. At NNLO QCD, the Drell–Yan-like corrections to WH production also give the bulk of the corrections to ZH production [81]. For ZH production there are, however, gluon-gluon induced contributions that do not involve a virtual Z gauge boson but are such that the Z gauge boson and H boson couple to gluons via top-quark loops [82], see diagram (d) in Fig. 11.1. NLO QCD virtual corrections to the partonic cross section for $gg \to ZH$, in the high-energy and large top mass limits are available in Refs. [83]. In addition, WH and ZH production receive non Drell–Yan-like corrections in the $q\bar{q}'$ and $q\bar{q}$ initiated channels, respectively, at the NNLO level in QCD, where the Higgs boson is radiated off top-quark loops [84]. The full QCD corrections up to NNLO order, the NLO EW corrections and the NLO corrections to the gluon-gluon channel are available in `VH@NNLO` [85]. NNLO QCD corrections to $pp \to WH$+jet are important for signal modelling. NLO corrections to cross section inclusive in the number of jets show excellent convergence while NNLO QCD corrections to exclusive single jet cross section are much more significant [86].

As neither the Higgs boson nor the weak gauge bosons are stable particles, their decays also have to be taken into account. Providing full kinematical information for the decay products can furthermore help in the suppression of large QCD backgrounds. Differential distributions for the processes $pp \to WH \to \bar{\nu}_\ell \ell H$ and $pp \to ZH \to \ell^+\ell^- H/\nu_\ell \bar{\nu}_\ell H$, including NLO QCD and EW corrections, have been presented in Ref. [87]. The NNLO QCD corrections to differential observables for WH production at the LHC, including the leptonic decays of the W boson and the decay of the Higgs boson into a $b\bar{b}$ pair, are presented in Ref. [88]. Calculations at the same level, including also the ZH process have been performed [89]. The WH production mode has also been matched to a parton shower at NNLO QCD accuracy [90]. Full NNLO QCD results for both the production and decay are available [91] and show a large impact of radiation from the final-state bottoms. The WH and ZH production modes, especially in the boosted regime, provide a relatively clean environment for studying the decay of the Higgs boson into bottom quarks [92]. Bottom mass effects have been computed at NNLO [93,94] and tend to increase the rates by 6-7%.

The inclusive cross section for associated Higgs boson production with a massive gauge boson is recently known up to N3LO QCD too [95].

iv. *Higgs boson production in association with $t\bar{t}$*

Higgs boson radiation off top quarks, $pp \to t\bar{t}H$, provides a direct probe of the top-Higgs Yukawa coupling. The LO cross section for this production process was computed in Ref. [96]. Later, the NLO QCD [97] and NLO EW corrections [98] were evaluated yielding a moderate increase in the total cross section of at most 20%, but significantly reducing the scale dependence of the inclusive cross section. The EW corrections can be enhanced by large electroweak Sudakov logarithms in particular in the boosted regime often used in the phenomenological analyses [99]. The resummation of soft gluon contributions close to the partonic kinematical threshold are considered in Refs. [100] to reach a result at NLO+NNLL QCD order. Full off-shell calculations with decaying top quarks are computed at NLO QCD [101] and NLO QCD + EW [102] order, respectively. The fixed-order NLO QCD calculation has been interfaced with the standard parton shower Monte-Carlo generators